Supporting Information

Doping-induced grain refinement contributes to enhanced thermoelectric performance of *n*-type PbSe at room temperature

Canyang Zhao,‡[a] Qian Deng,‡[a] Wei Yuan,[a] Xiang An,[a] Wenjun Su,[a] Zhengmin He,[a] Yin Xie,[a] Zhilong Zhao[a] and Ran Ang*[a,b]

[a] *Key Laboratory of Radiation Physics and Technology, Ministry of Education, Institute of Nuclear Science and Technology, Sichuan University, Chengdu 610064, China*

[b] *Institute of New Energy and Low-Carbon Technology, Sichuan University, Chengdu 610065, China*

‡ C. Zhao and Q. Deng contributed equally to this work.

*Corresponding author and Email: rang@scu.edu.cn

Experimental section

Sample synthesis

High-purity Pb (99.999%, particles, Zhongnuo), Se (99.999%, particles, Zhongnuo), Ge (99.999%, particles, Zhongnuo), Cu (99.999%, particles, Zhongnuo), and S (99.999%, particles, Zhongnuo) were weighed according to the nominal composition $(Pb_{0.995}Sb_{0.005}Se)_{1-x}(GeS)_x$ (x = 0-0.12) and $Cu_y(PbSe)_{0.9}(GeS)_{0.1}$ (y = 0.002-0.005) and placed into quartz tubes, which were flame-welded at 10^{-4} Torr. These mixed particles were treated by melting–quenching by slowly raising to 1423 K, holding for 6 hours and subsequently quenching and cooling using ice-water. To enhance the stability of the samples, the quenched ingots were annealed at 873 K for 48 hours. The obtained products were hand-ground in an agate motar for 10 minutes to a fine powder, and then densified by the hot pressing (HP) method at 923 K under a uniaxial pressure of 45 MPa for 25 minutes. After hot pressing, some cylindrical samples with a relative density of at least 96% and a diameter of 12.7 mm were obtained.

Materials Performance Characterization

The powder X-ray diffraction patterns were recorded with Cu $K\alpha$ radiation. Scanning electron microscope (SEM) equipped with energy-dispersive spectroscopy (EDS) was used to characterize surface morphology and qualitative and quantitative analysis of composition. The electrical conductivity σ and Seebeck coefficient S were measured by CTApro measurement system (Beijing Cryoall Science and Technology Co., Ltd. China). The Hall coefficient, which was closely related to carrier concentration and mobility, was measured using the van der Pauw technique under a reversible magnetic field of 1.5 T. The thermal conductivity (κ_{total}) was calculated by $\kappa=dC_pD$, where D is the thermal diffusivity measured by a laser flash technique with the Netzsch LFA467 system, C_p is the heat capacity estimated by $C_p(k_B/atom)=3.07+4.7(T/K-300)/10000$.[1,2] Ignoring the bipolar thermal conductivity (κ_{bip}), the lattice thermal conductivity (κ_l) was directly obtained by subtracting the electronic conductivity (κ_e) from the κ_{total}, the κ_e was calculated by the Wiedemann-Franz relationship, $\kappa_e = LT/\rho$, where L is the Lorentz number.[3] L was derived with the single parabolic band (SPB) model.[4]

Computational details

Electrical transport modeling

The density of state mass m* and Lorenz number L were calculated based on single parabolic band (SPB) model by the following equations[5]:

$$S = \frac{k_b}{e}\left[\frac{(r+5/2)F_{r+3/2}(\eta)}{(r+3/2)F_{r+1/2}(\eta)} - \eta\right] \quad \text{(eq. S1)}$$

$$n_H = \frac{4\pi}{A}\left[\frac{2m^* k_B T}{h^2}\right]^{3/2} F_{1/2}(\xi) \quad \text{(eq. S2)}$$

$$A = \frac{3}{2}F_{1/2}(\eta)\frac{F_{-1/2}}{2F_0^2} \quad \text{(eq. S3)}$$

$$L = \frac{\kappa_B^2 3F_0F_2 - 4F_1^2}{e^2F_0^2}$$

(eq. S4)

$$F_n(\xi) = \int_a^{\infty} \frac{x^n}{1 + e^{(x-\xi)}} dx$$

(eq. S5)

Here, k_B is the Boltzmann constant, F_n is the Fermi integral, and the reduced chemical potential is given by $\xi = E_F/(k_BT)$, where E_F is the Fermi energy.

Thermal transport modeling

The lattice thermal conductivity (κ_L) of alloys was calculated by the modified Debye-Callaway model,[6] which can be expressed by the equation (6).

$$\kappa_{lat} = \frac{K_B}{2\pi^2 v}\left(\frac{K_B}{\hbar}\right)^3 \int_0^{\Theta/T} \tau_{tot}(x) \frac{x^4 e^x}{(e^x - 1)^2} dx$$

(eq. S6)

Here, v is the average speed of phonon, $\hbar$ is the reduced Planck constant, Θ is the Debye temperature, x is the relation of $\hbar\omega/k_BT$, ω is the phonon frequency, and τ_{tot} is the total phonon scattering relaxation time. τ_{tot} can be attributed to scattering from various mechanisms such as normal (N) and Umklapp (U) processes, point defects (PD), nanoprecipitates (NP), boundaries (B), dislocation cores (DC), and dislocation strains (DS) according to the Matthiessen's equation $\tau_{tot}^{-1} = \tau_U^{-1} + \tau_N^{-1} + \tau_{PD}^{-1} + \tau_{NP}^{-1} + \tau_B^{-1} + \tau_{DS}^{-1} + \tau_{DC}^{-1}$. The phonon scattering relaxation time for respective mechanism can be expressed as follows:

Umklapp phonon scattering

$$\tau_U^{-1} = A_N * \frac{2K_B \bar{V}^{1/3} \omega^2 \gamma^2 T}{(6\pi^2)^{\frac{1}{3}} \bar{M} v^3}$$

(eq. S7)

Normal phonon scattering

$$\tau_N^{-1} = \frac{2K_B \bar{V}^{1/3} \omega^2 \gamma^2 T}{(6\pi^2)^{\frac{1}{3}} \bar{M} v^3}$$

(eq. S8)

Point defect phonon scattering

$$\tau_{PD}^{-1} = \frac{\bar{V}_\omega^4}{4\pi^3 v^3} * \sum (1 - x_i)\left[\left(\frac{M_i - M}{M}\right)^2 + \varepsilon\left(\frac{a_i - a}{a}\right)^2\right]$$

(eq. S9)

Precipitates scattering

$$\tau_{NP}^{-1} = v(\sigma_s^{-1} + \sigma_L^{-1})^{-1} V_p$$

(eq. S10)

Boundaries scattering[7]

$$\tau_B^{-1} = \frac{v}{d}$$

(eq. S11)

Dislocation scattering that includes both dislocation core (τ_{DC}) and dislocation strain(τ_{DS}) scattering.

$$\tau_{DC}^{-1} = N_D \frac{\overline{V}^{4/3}}{v^2} \omega^3$$

(eq. S12)

$$\tau_{DS}^{-1} = A' N_D \gamma^2 B_D^2 \omega \left\{ \frac{1}{2} + \frac{1}{24} \left(\frac{1-2v}{1-v} \right)^2 \left[1 + \sqrt{2} \left(\frac{v_L}{v_T} \right)^2 \right] 2 \right\}$$

(eq. S13)

In above equations, $\overline{V}$ is the average atomic volume, $\overline{M}$ is the average atomic mass, γ is the Grüneisen parameter, A_N is the ratio between normal process and Umklapp phonon scattering, N_D is the number of dislocations (or stacking faults) crossing a line of unit length, B_D is the magnitude of the Burgers vector of the dislocation.

Supplementary Figures

Figure S1. Crystal structure. Room temperature lattice parameters for (a) $(Pb_{0.995}Sb_{0.005}Se)_{1-x}(GeS)_x$ and (b) $Cu_y(PbSe)_{0.9}(GeS)_{0.1}$ samples.

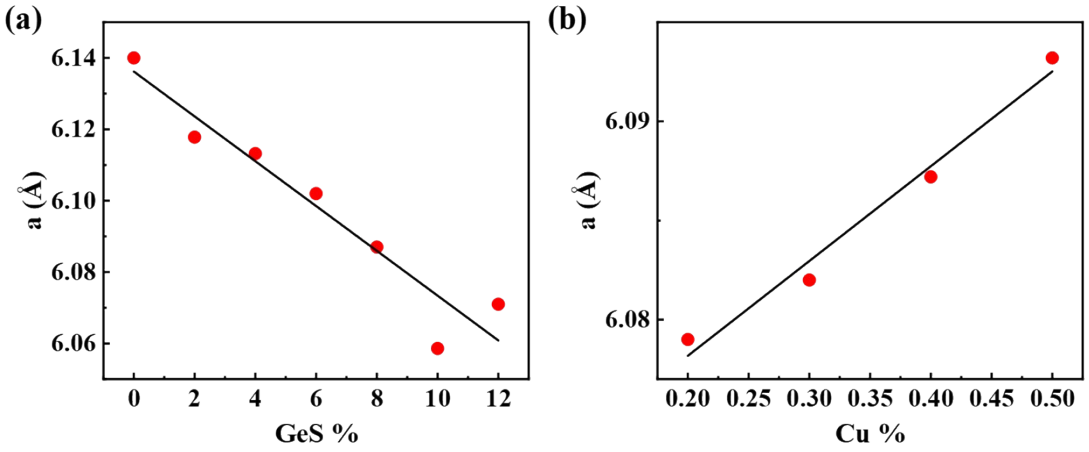

Figure S2. The back-scattered electron image and corresponding energy dispersive x-ray spectroscopy (EDS) mapping for (a) $Pb_{0.995}Sb_{0.005}Se$ and (b) $(Pb_{0.995}Sb_{0.005}Se)_{0.9}(GeS)_{0.1}$ samples.

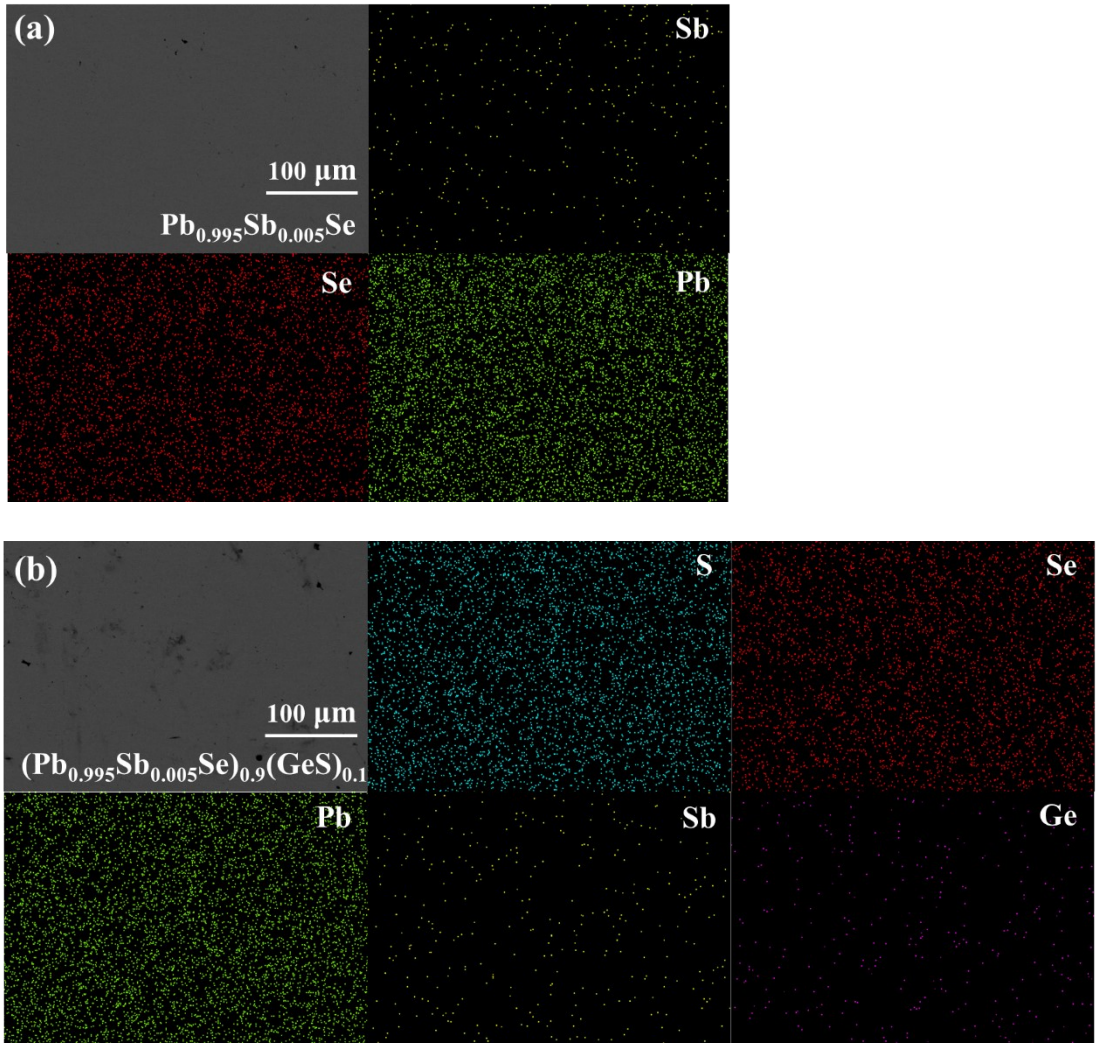

Figure S3. The grain boundary of $Cu_{0.004}(PbSe)_{0.9}(GeS)_{0.1}$ sample and corresponding EDS line scan.

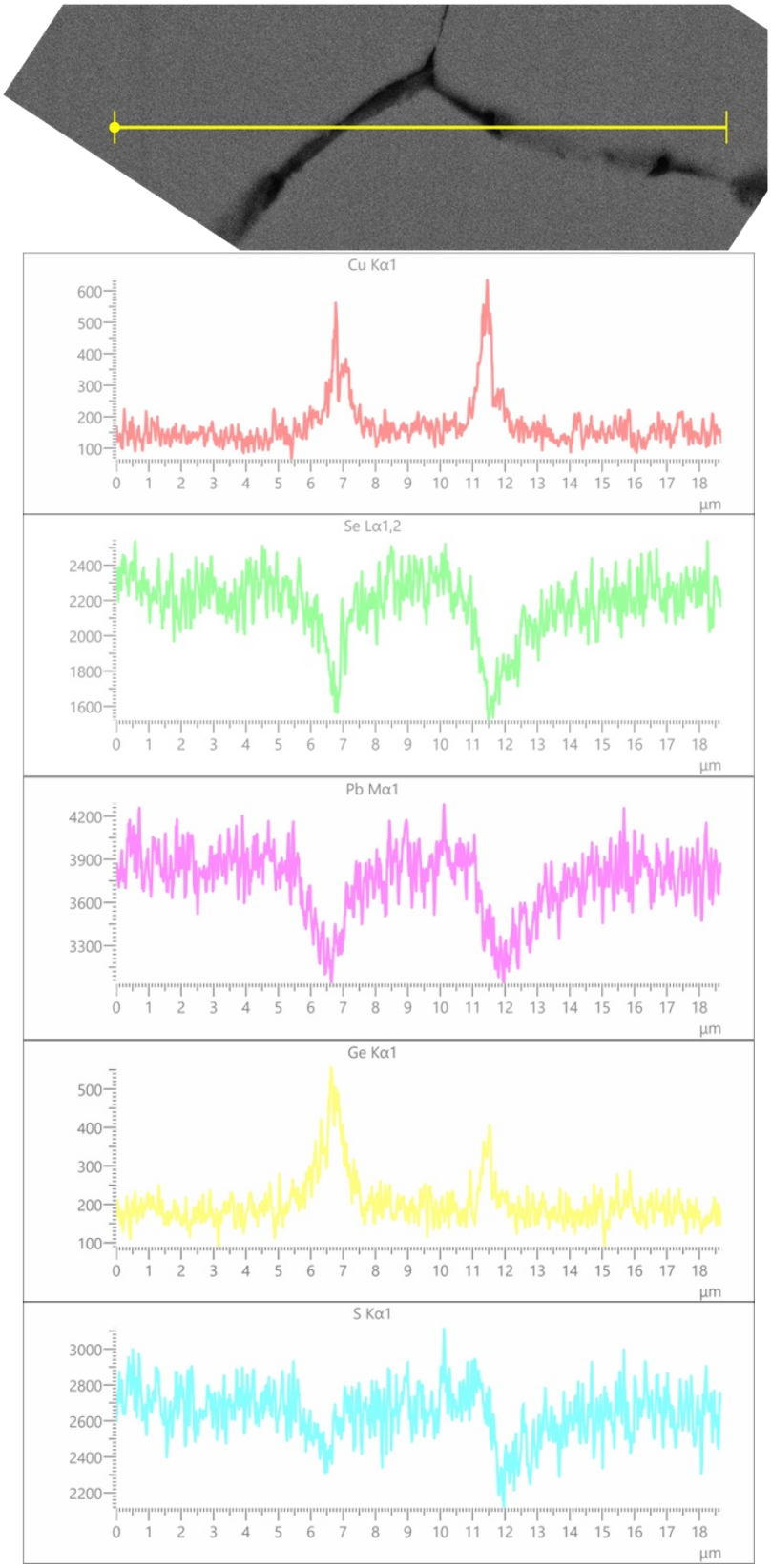

Figure S4. (a) The carrier concentration n and carrier mobility μ_H in room temperature. (b) The temperature dependent lattice thermal conductivity κ_L.

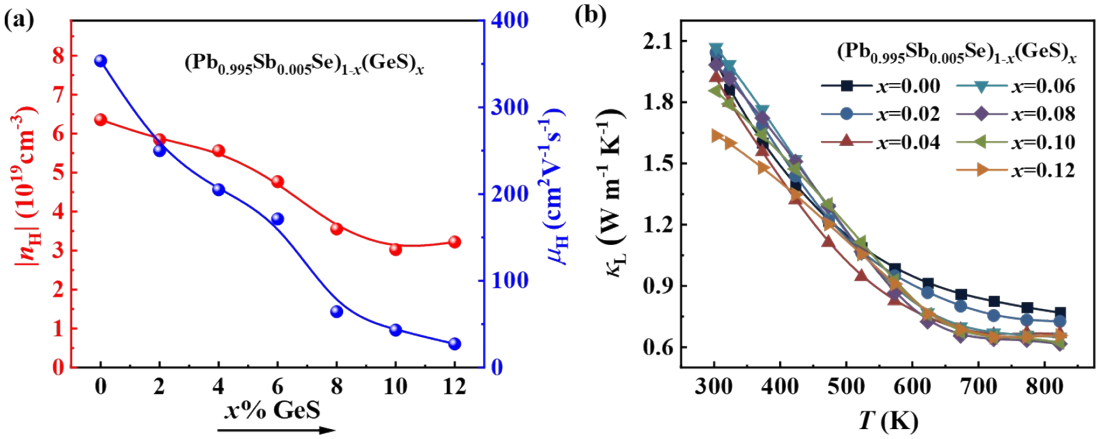

Figure S5. The room-temperature Hall carrier mobility and concentration of $Cu_y(PbSe)_{0.9}(GeS)_{0.1}$ compared with $(Pb_{0.995}Sb_{0.005}Se)_{0.9}(GeS)_{0.1}$.

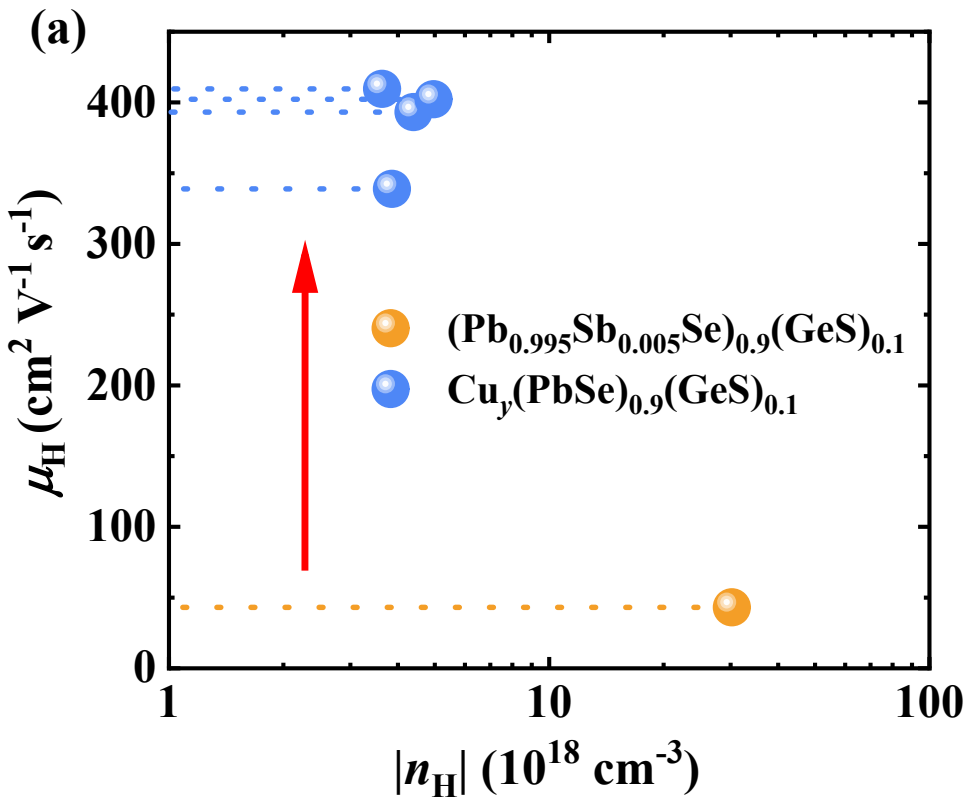

Figure S6. The thermal diffusivity and heat capacity of $Cu_y(PbSe)_{0.9}(GeS)_{0.1}$ and $(Pb_{0.995}Sb_{0.005}Se)_{1-x}(GeS)_x$.

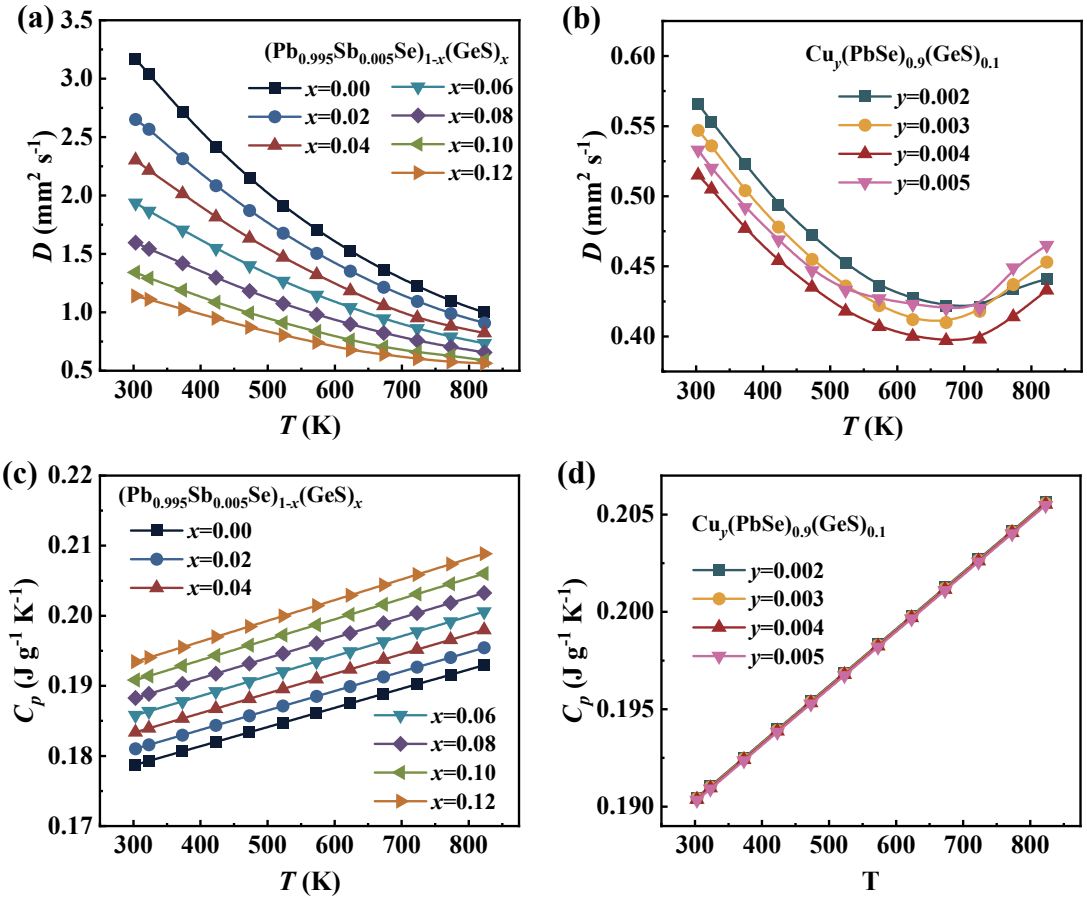

Figure S7. The Grain size frequency distribution histogram of $(Pb_{0.995}Sb_{0.005}Se)_{0.9}(GeS)_{0.1}$ and $Cu_{0.004}(PbSe)_{0.9}(GeS)_{0.1}$.

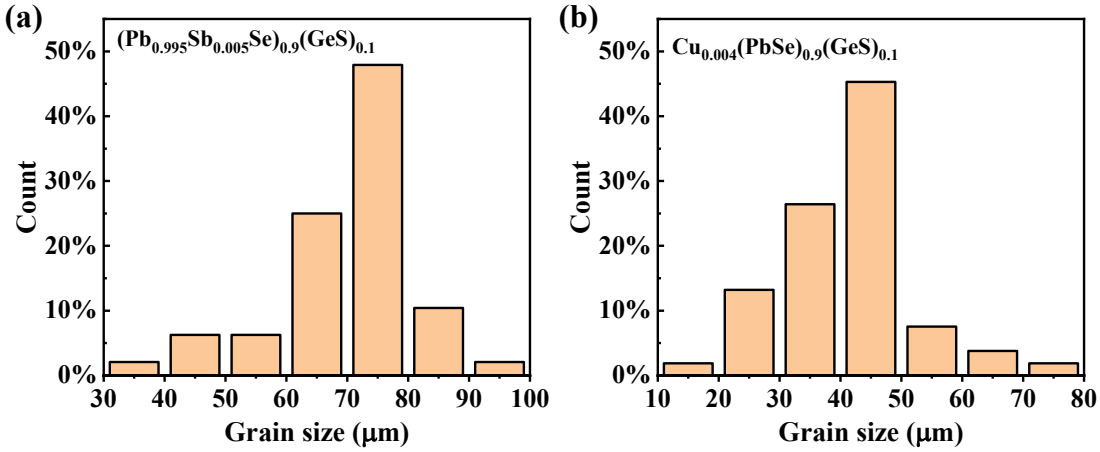

Figure S8. The thermoelectric properties of $(PbSe)_{0.9}(GeS)_{0.1}$: (a) electrical conductivity, σ; (b) Seebeck coefficient, S; (c) total, electrical and lattice thermal conductivity, κ_{tot}, κ_{ele} and κ_{lat}; (d) figure of merit, zT.

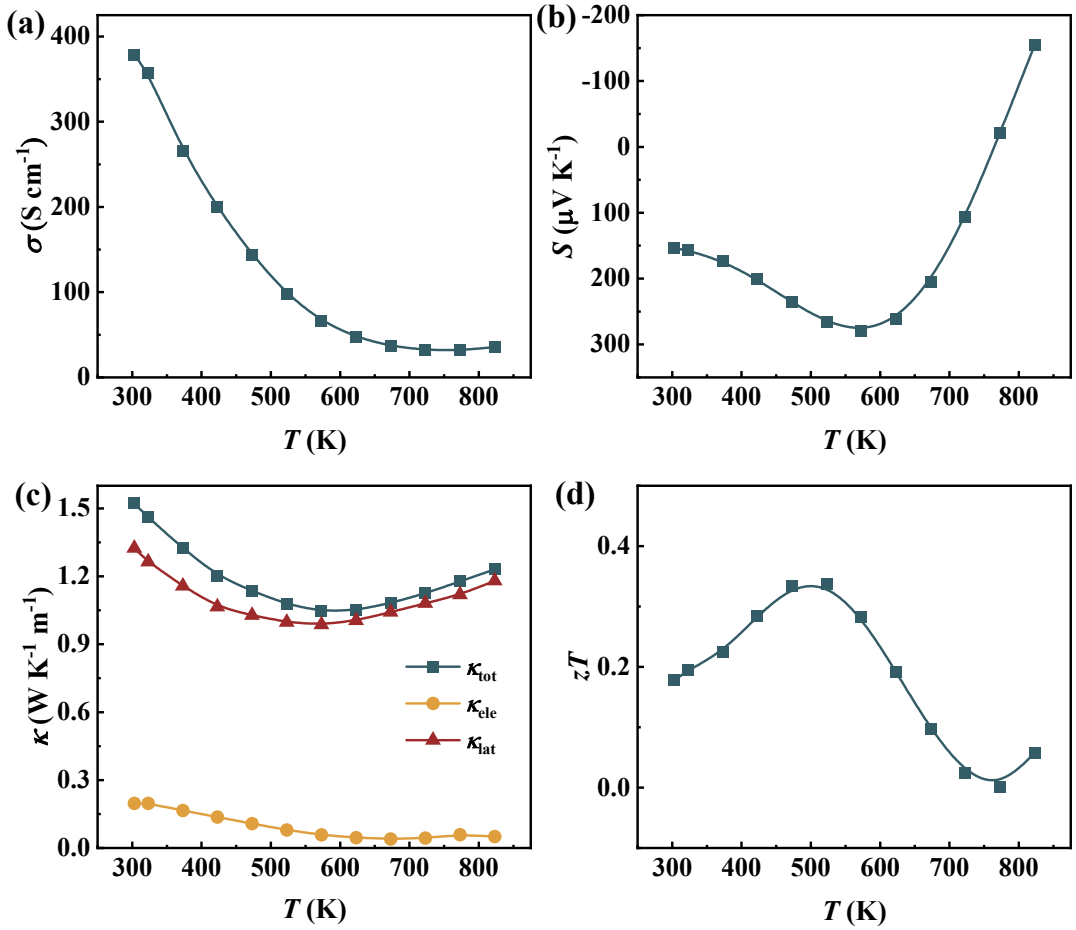

Supplementary Tables

Table S1. Parameters adopted in the Debye-Callaway Model Simulation.

Parameters	Values
Lattice constant a,b and c (Å)	a,b,c=6.085
Average atomic mass M (kg)	2.2274×10^{-25}
Average atomic mass volume V_0 (m^3)	2.8625×10^{-29}
Boltzmann constant K_B (J/K)	1.38×10^{-23}
Grüneisen parameter γ	1.7[8]
Point defect scattering parameter Γ	1.9477×10^{-1}
Average sound velocity ν (m/s)	2614[9]
Longitudinal velocity ν_L (m/s)	3150[9]
Transverse velocity ν_T (m/s)	1600[9]
Debye temperature Θ (K)	139[10]
Ratio of N- to U- processes β	4[11]
Phenomenological parameter ε_i	64[12]

Table S2. The density of $Cu_y(PbSe)_{0.9}(GeS)_{0.1}$ and $(Pb_{0.995}Sb_{0.005}Se)_{1-x}(GeS)_x$.

Sample	Density (g cm^{-3})
$Cu_{0.002}(PbSe)_{0.9}(GeS)_{0.1}$	7.711
$Cu_{0.003}(PbSe)_{0.9}(GeS)_{0.1}$	7.701
$Cu_{0.004}(PbSe)_{0.9}(GeS)_{0.1}$	7.664
$Cu_{0.005}(PbSe)_{0.9}(GeS)_{0.1}$	7.651
$Pb_{0.995}Sb_{0.005}Se$	8.282
$(Pb_{0.995}Sb_{0.005}Se)_{0.98}(GeS)_{0.2}$	8.134
$(Pb_{0.995}Sb_{0.005}Se)_{0.96}(GeS)_{0.4}$	8.057
$(Pb_{0.995}Sb_{0.005}Se)_{0.94}(GeS)_{0.6}$	7.996
$(Pb_{0.995}Sb_{0.005}Se)_{0.92}(GeS)_{0.8}$	7.921
$(Pb_{0.995}Sb_{0.005}Se)_{0.9}(GeS)_{0.1}$	7.819
$(Pb_{0.995}Sb_{0.005}Se)_{0.88}(GeS)_{0.12}$	7.769

References:

1. R. Blachnik and R. Igel, *Zeitschrift für Naturforschung B*, 1974, **29**, 625-629.
2. Y. Pei, X. Shi, A. LaLonde, H. Wang, L. Chen and G. J. Snyder, *Nature*, 2011, **473**, 66-69.
3. H.-S. Kim, Z. M. Gibbs, Y. Tang, H. Wang and G. J. Snyder, *APL Mater.*, 2015, **3**, 041506.
4. M. Hong, Y. Wang, S. Xu, X. Shi, L. Chen, J. Zou and Z.-G. Chen, *Nano Energy*, 2019, **60**, 1-7.
5. Y. I. Ravich, B. Efimova and V. Tamarchenko, *physica status solidi (b)*, 1971, **43**, 11-33.
6. J. Callaway and H. C. von Baeyer, *Physical Review*, 1960, **120**, 1149.
7. D. Morelli, J. Heremans and G. Slack, *Phys. Rev. B*, 2002, **66**, 195304.
8. T. Grandke, M. Cardona and L. Ley, *Solid State Commun.*, 1979, **32**, 353-356.
9. Z. Chen, B. Ge, W. Li, S. Lin, J. Shen, Y. Chang, R. Hanus, G. J. Snyder and Y. Pei, *Nat. Commun.*, 2017, **8**, 13828.
10. Z.-Z. Luo, S. Hao, X. Zhang, X. Hua, S. Cai, G. Tan, T. P. Bailey, R. Ma, C. Uher, C. Wolverton, V. P. Dravid, Q. Yan and M. G. Kanatzidis, *Energy Environ. Sci.*, 2018, **11**, 3220-3230.
11. H. Wang, Y. Pei, A. D. LaLonde and G. J. Snyder, *Proceedings of the National Academy of Sciences of the United States of America*, 2012, **109**, 9705-9709.
12. H. Wang, J. Wang, X. Cao and G. J. Snyder, *J. Mater. Chem. A*, 2014, **2**, 3169-3174.